Journal of Electron Spectroscopy and Related Phenomena 195 (2014) 231–236

Journal of Electron Spectroscopy and Related Phenomena

journal homepage: www.elsevier.com/locate/elspec

Time- and angle-resolved photoemission spectroscopy with optimized high-harmonic pulses using frequency-doubled Ti:Sapphire lasers

S. Eich[a], A. Stange[b], A.V. Carr[c], J. Urbancic[a], T. Popmintchev[c], M. Wiesenmayer[a], K. Jansen[b], A. Ruffing[a], S. Jakobs[a], T. Rohwer[b], S. Hellmann[b], C. Chen[c], P. Matyba[c], L. Kipp[b], K. Rossnagel[b], M. Bauer[b], M.M. Murnane[c], H.C. Kapteyn[c], S. Mathias[a,c,*], M. Aeschlimann[a]

[a] University of Kaiserslautern and Research Center OPTIMAS, 67663 Kaiserslautern, Germany
[b] Institute of Experimental and Applied Physics, University of Kiel, D-24098 Kiel, Germany
[c] JILA, University of Colorado and NIST, Boulder, CO 80309-0440, USA

ARTICLE INFO

Article history:
Available online 22 May 2014

Keywords:
Time-resolved photoemission spectroscopy
Extreme-ultraviolet photoemission spectroscopy
Femtosecond dynamics
Two-photon photoemission
Time-resolved ARPES

ABSTRACT

Time- and angle-resolved photoemission spectroscopy (*tr*ARPES) using femtosecond extreme ultraviolet high harmonics has recently emerged as a powerful tool for investigating ultrafast quasiparticle dynamics in correlated-electron materials. However, the full potential of this approach has not yet been achieved because, to date, high harmonics generated by 800 nm wavelength Ti:Sapphire lasers required a trade-off between photon flux, energy and time resolution. Photoemission spectroscopy requires a quasi-monochromatic output, but dispersive optical elements that select a single harmonic can significantly reduce the photon flux and time resolution. Here we show that 400 nm driven high harmonic extreme-ultraviolet *tr*ARPES is superior to using 800 nm laser drivers since it eliminates the need for any spectral selection, thereby increasing photon flux and energy resolution to <150 meV while preserving excellent time resolution of about 30 fs.

1. Introduction

Angle-resolved photoemission spectroscopy (ARPES) using synchrotron radiation in the extreme ultraviolet (XUV) region of the spectrum is one of the most powerful techniques used to study the electronic properties of surfaces, interfaces and correlated-electron materials over the last decade [1–3]. ARPES can measure the energy-versus-momentum electronic structure including the Fermi surface. It also yields information about many-body effects since the energy and momentum dependent photocurrent often reflects the single-particle spectral function. More recently, by combining ARPES with the ultrahigh time resolution of femtosecond lasers, new frontiers in capturing the fastest processes relevant to function in materials and at surfaces have been explored. One pioneering experiment that illustrated the potential of time- and angle-resolved photoemission (*tr*ARPES) for studying correlated-electron materials was carried out by Schmitt et al. in 2008, probing the photo-induced charge-density-wave phase transition in $TbTe_3$ in real time [4]. A series of experiments soon followed, where ultrafast ARPES spectroscopy was used to separate timescales in order to probe the complex and correlated interactions between charges, spins, orbitals and the crystal lattice [5–8]. Until recently, however, *tr*ARPES experiments used low-energy ultrafast laser pulses in the visible and UV region of the spectrum (up to 7 eV). This limits the accessible energy and momentum space to about ≈2 eV below the Fermi level and ≈0.5 $Å^{-1}$, respectively. In comparison, typical band structures span ≈5 eV, with Brillouin zone boundaries extending to ≈1.5 $Å^{-1}$.

Extending *tr*ARPES into the extreme ultraviolet (XUV) and soft X-ray regions of the spectrum can overcome these limitations of visible/UV laser based approaches [9–21], an approach that was pioneered by Richard Haight starting in 1989 [10]. Tabletop high-harmonic sources, in combination with time-of-flight photoemission spectroscopy, had long been used to probe charge dynamics in organic and semiconducting materials, as well as in adsorbates [22,23]. By using ultrafast high-harmonic generation (HHG) in combination with ARPES in 2007, we demonstrated

* Corresponding author at: University of Kaiserslautern and Research Center OPTIMAS, 67663 Kaiserslautern, Germany. Tel.: +49 631 205 3576.
E-mail address: smathias@physik.uni-kl.de (S. Mathias).

http://dx.doi.org/10.1016/j.elspec.2014.04.013

decent quality static ARPES spectra on metals and quantum wells [17,24]. Recently, Rohwer et al. used HHG-based ARPES with a state-of-the-art parallel detection scheme to measure the photoinduced suppression of a charge-ordered state in the potential excitonic insulator 1*T*-$TiSe_2$ [13]. Petersen et al. used this technique to measure the melting transition of charge and lattice order in 1*T*-TaS_2 [15]. In 2012, Hellmann et al. demonstrated that *tr*ARPES can in general directly measure the quenching times of electronic order parameters and thus identify, via systematic temporal discrimination of elementary electronic and structural processes, the dominant interactions in correlated electron materials [14]. Also in 2012, Carley et al. succeeded to map the transient valence band structure of Gd in an ultrafast demagnetization process [16]. For a comprehensive reviews of high-harmonic radiation in surface science, see Refs. [18,25,26]. Nevertheless, despite the great success of these time-resolved XUV photoemission experiments, the quasi-monochromatic source requirements impose a trade-off between HHG photon flux, energy, and time resolution.

Here we present a method to overcome these limitations. Specifically, we use the second harmonic (2ω) of a Ti:Sapphire laser at a fundamental wavelength of 780 nm to generate an isolated bright 7th high harmonic at 22.3 eV. This harmonic can then be used for *tr*ARPES with 150 meV energy and 30 fs time resolution, *without any trade-off in the XUV photon flux*. Moreover, because of the additionally large (6.4 eV) spectral separation of odd-order harmonics when driven by 2ω (3.2 eV) beams [21,27], we can omit all dispersive optical elements in the XUV beamline. Thus, no monochromator is needed that might degrade the XUV pulse length and reduce the high harmonic flux. Instead, we directly use the intrinsic harmonic structure generated within the HHG process. Additionally, for shorter wavelength driving lasers, the HHG process is more efficient, so that lower pump intensity is needed to achieve high photon flux in the XUV [21,28,29]. This approach is therefore well-suited for *tr*ARPES and will also be useful for other advanced spectroscopies using HHG such as cold target recoil ion momentum spectroscopy (COLTRIMS) [30–32], velocity-map imaging (VMI) [33], magneto-optical experiments [34–36], as well as HHG-based coherent diffractive imaging (CDI) applications [9].

2. Experiment

2.1. XUV trARPES with HHG light pulses

In high-harmonic generation, an intense femtosecond laser beam is focused into a noble gas, thus generating a train of attosecond XUV bursts that are emitted each half-cycle of the driving laser field (see Fig. 1a). To a first approximation, the spectrum of a single attosecond burst within one half-cycle of the driving laser is an XUV continuum up to a maximum photon energy that is determined by the laser intensity and laser wavelength [37]. To generate discrete peaks appropriate for high-resolution ARPES, the HHG process can be driven by multicycle laser pulses, as shown in Fig. 1a. The periodic HHG emission in time gives rise to a periodic emission in frequency, thereby creating a spectrum of odd harmonics, spaced by two times the fundamental driving laser energy (Fig. 1b). The bandwidth of the HHG emission ($\Delta\omega$) is related to the pulse length of each attosecond burst (Δt) by a time-bandwidth product. The bandwidth of the individual harmonics ($\delta\omega$) is antiproportional to the pulse length of the HHG attosecond pulse train (APT, see Fig. 1) (δt) and therefore also to the pulse length of the fundamental laser that drives the HHG process.

Generating bright harmonics requires that the frequency upconversion process be phase matched [38]. When macroscopic phase matching is achieved, the laser and high-order nonlinear polarization propagate in phase (at the speed of light c) throughout the medium so that the HHG signals from many atomic emitters add coherently. Phase matching is achieved by balancing the neutral gas ($n > 1$) and free-electron plasma dispersion ($n < 1$) that is created as the medium is ionized by the strong electric field of the driving laser pulse. In a gas-filled capillary waveguide, this phase matching is achieved by adjusting the gas pressure. This geometry has also the advantage of a long phase matching region and efficient differential pumping after the capillary, minimizing reabsorption of the generated harmonics and allowing for coupling to an ultrahigh vacuum chamber.

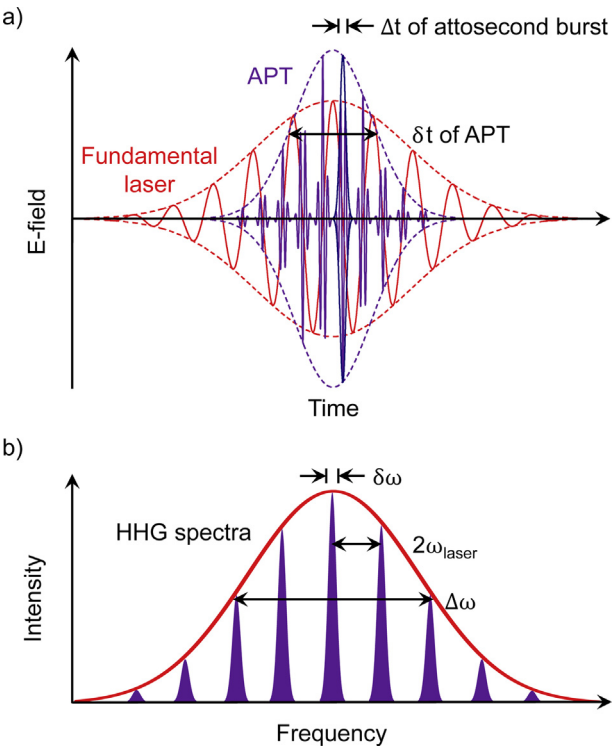

Fig. 1. Phase matched high-harmonic generation in a multicycle driving laser field. The figure illustrates the relationship between (a) the time duration of the individual attosecond burst (Δt) and the full attosecond pulse train "APT" (δt) to (b) the spectral bandwidth of the HHG comb ($\Delta\omega$) and the spectral width ($\delta\omega$) of an individual harmonic.

For many applications in ARPES, COLTRIMS or CDI, a single bright and narrow-band harmonic is required, which is usually achieved by using a pair of XUV mirrors or a (grating) monochromator [22,39–41]. Ideally, for time-resolved experiments, the output would be adjustable and time-bandwidth limited. However, most single-grating monochromators introduce significant temporal dispersion and have low throughput (<30%) [16,42]. Double-grating time-compensated monochromators that do not provide this temporal dispersion result in even lower throughput (<20%) [43]. Alternatively, narrow band XUV mirrors must trade off reflectivity (from ≈10% to ≈70% for each mirror depending on XUV wavelength) to achieve a relatively narrow bandwidth of <1 eV. In the following, we demonstrate how both the intrinsic structure of the harmonics in the energy and time domain, and the photon flux, can be optimized simultaneously so that monochromatizing optical elements become unnecessary.

2.2. Experimental setup for XUV trARPES

Fig. 2 shows the experimental realization of our *tr*ARPES setup using optimized and bright XUV light pulses. The majority (95%) of the output of a single-stage, cryocooled, Ti:Sapphire multipass laser amplifier system [44] operating at 10 kHz, 1.2 mJ, 25 fs, 780 nm is

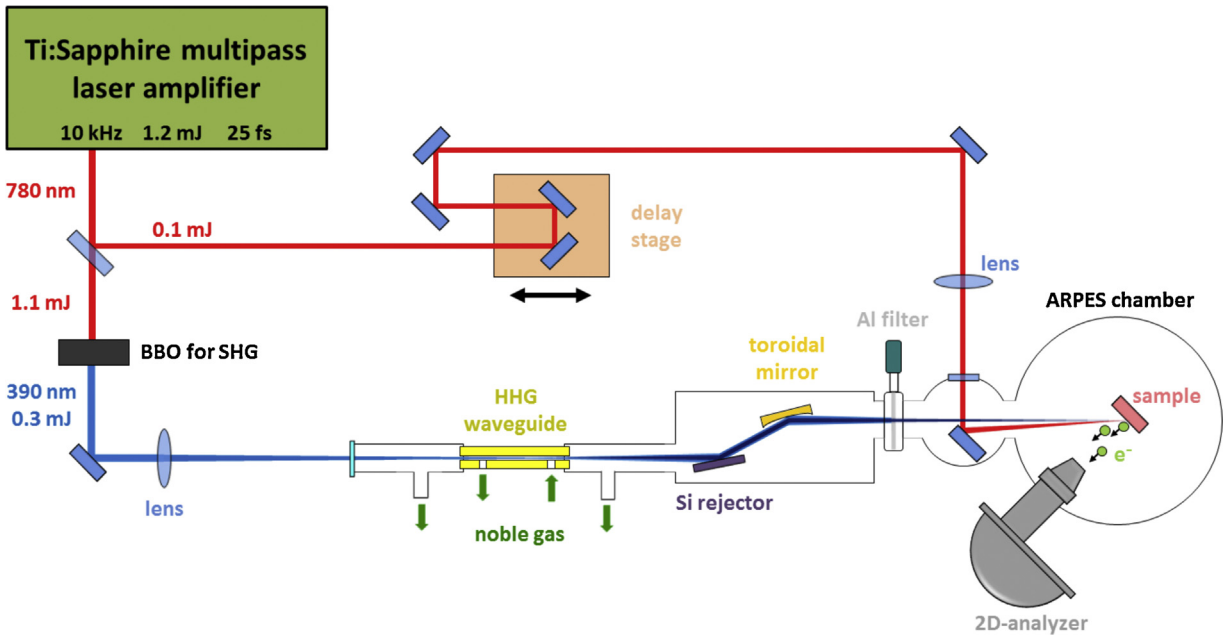

Fig. 2. Experimental realization of the *tr*ARPES setup with optimized and bright XUV pulses. For the measurements presented in Fig. 3, the UHV chamber was replaced with an XUV spectrometer consisting of a grating and a multi-channel plate.

used to generate the second harmonic in a 200 μm thick beta barium borate (BBO) crystal, which yields pulses at 390 nm with 300 μJ energy per pulse. Note that we do not compensate for dispersion after the frequency doubling process, since we deliberately want to drive the HHG process with longer pulses in order to reduce the bandwidth of the individual harmonics [45]. After frequency doubling and focusing, we estimate a pulse length of 35–40 fs (transform limit of 30 fs and positive chirp of ~200 fs^2) for the 390 nm pulses. We focus the blue light (which is separated from the fundamental light with a dichroic mirror) into a 5 cm long, 150 μm inner-diameter capillary waveguide [38,46] filled with 15–20 Torr of Kr gas (see Fig. 3b), where we dominantly generate the 7th harmonic at 22.3 eV (as shown in Fig. 3a, discussed below). We use a Si wafer to reflect the generated HHG light (while rejecting much of the laser light) onto a toroidal mirror, which is then used to focus the HHG beam onto the sample in the UHV chamber. The residual blue light is blocked using a 200 nm thick Al filter. For the results presented in Fig. 3, the UHV chamber was replaced with an XUV spectrometer consisting of a grating and multi-channel plate.

2.3. Optimization of the HHG output for XUV trARPES

2.3.1. Elimination of monochromatizing elements

Our first goal for optimized *tr*ARPES with XUV pulses is to maintain bright high harmonic flux and short pulse duration. Dispersive optical elements in the XUV beamline can increase loss and cause HHG pulse broadening, so that ideally, we would omit these optics entirely and work with the direct output of the HHG light source. Fortunately, this can be accomplished very naturally using HHG driven by blue 390 nm lasers. Typically, when the fundamental of a Ti:Sapphire amplifier system is used for HHG (centered around ≈780 nm, and corresponding to a photon energy of ≈1.6 eV) the odd harmonic spacing is ≈3.2 eV. Considering a photoemission spectrum recorded with 3.2 eV spaced multiple harmonics lead to overlapping replicas of the electronic structure of the sample that are energetically separated by the 3.2 eV, unless a single harmonic is used. Typical band structures in materials, in comparison, extend over an energy range of $\Delta E \approx 5$ eV below the Fermi level. Therefore, the replicated photoemission spectra

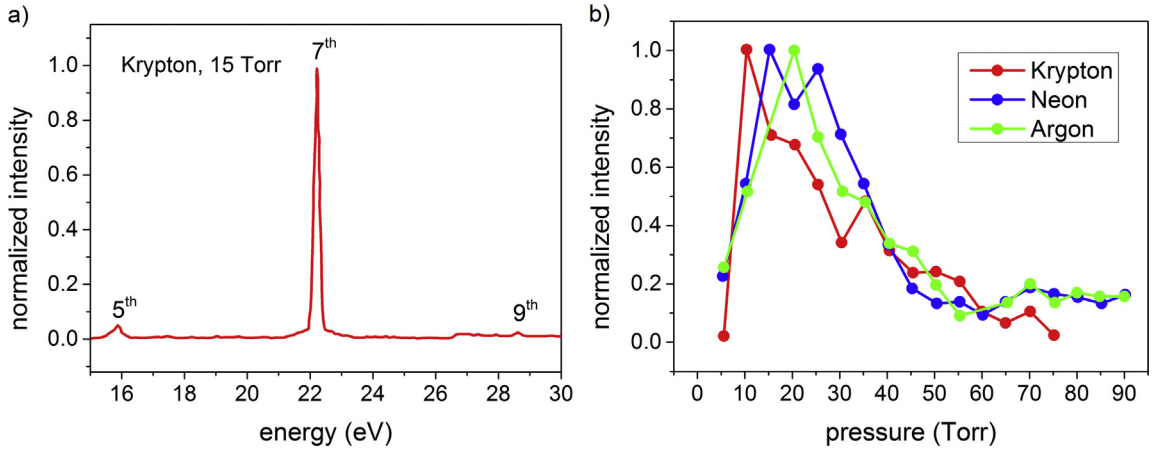

Fig. 3. Characterization of the HHG output pumped with the second harmonic of the Ti:Sapphire amplifier. (a) 390 nm-generated HHG spectrum in 15 Torr Kr and (b) phase-matching pressure scan for 390 nm-generated harmonics in Ne, Kr, and Ar. (For interpretation of the references to color in this text, the reader is referred to the web version of the article.)

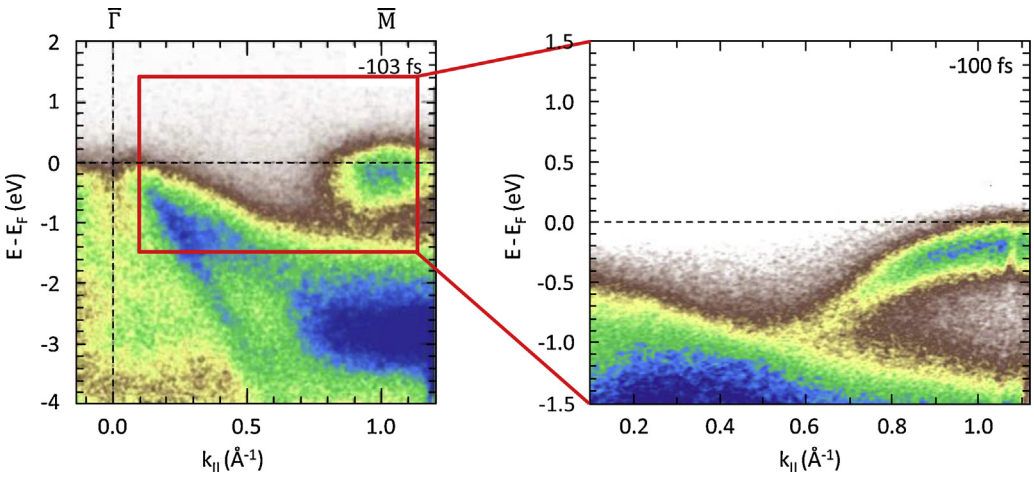

Fig. 4. Comparison of photoemission maps from $TiSe_2$ as recorded with our previous HHG setup with 780 nm HHG driving laser and an energy resolution of about 400 meV (c.f. Rohwer et al. [13], but note that different photoemission cross-sections influence the spectrum), left, and after optimization of the HHG output for an increased energy resolution, right, of <150 meV at optimal operation conditions.

will strongly overlap. This is even more critical if one additionally wants to monitor pump-induced electronic excitations from above the Fermi level. This problem can be solved, however, by using higher harmonics of Ti:Sapphire lasers to drive the HHG process. For example, the corresponding harmonic spacing for the second harmonic of Ti:Sapphire centered at 390 nm is 2 * 3.2 eV = 6.4 eV. This separation is already sufficient for most materials to achieve well-separated electronic band structure replicas in the photoemission spectrum (c.f. Fig. 4, right spectrum). The use of even shorter wavelengths to drive the HHG process, even with different lasers, is of course also suitable [27].

Fig. 3a shows the HHG spectrum generated in 15 Torr of Kr gas pumped by the second harmonic of the Ti:Sapphire amplifier at 390 nm, for a 300 μJ pulse energy. Clearly, the harmonics are well separated, with a very strong signal around 22.3 eV (7th harmonic). Additionally, the 7th harmonic is distinct in comparison to the 5th and 9th harmonic, independent of the gas medium due to absorption and phase matching effects [28,29], i.e. the Al filter blocks intensity of the 5th harmonic, and the cut-off energy is just below the 9th harmonic. This intrinsic distinction is particularly useful, since it allows monitoring replica-free band structures *over the full accessible energy and momentum range*. If further distinction of the 7th harmonic is needed, which might be the case if time-of-flight delay line detectors are used, a combination of Al–Sn filters can be used [47].

Fig. 3b shows a pressure scan for the 7th harmonic in Ne, Ar, and Kr. We achieve the highest HHG photon flux at pressures around 15–20 Torr. For the details of HHG spectra with shorter wavelength driving lasers in fibers in comparison to previous works [48], which is not the main topic here, we refer the reader to Refs. [28,29].

2.3.2. Stable and narrow bandwidth HHG generation

Our second goal is to generate a stable and ideally time-bandwidth limited HHG spectrum, which is needed to accommodate the long spectral integration times and the high energy and temporal resolution desired for XUV photoemission spectroscopy. First, we note that the intrinsic harmonic spectral bandwidth and peak position depends on many factors, such as the chirp of the fundamental laser pulse used to generate the harmonics. Additionally, excessive laser intensity can lead to nonlinear effects such as self-phase modulation [49], spectral blue shifting [50], or self-compression of the pulse while propagating through the gas [51]. One way to suppress these effects is to use the minimum possible laser intensity that is needed to drive a HHG process, while increasing the spot size.

In general, however, we show here that by using a shorter wavelength driving laser, it is easier to maintain a bright, stable and time-bandwidth limited HHG output for *tr*ARPES. For shorter wavelengths and therefore higher frequencies, the reduced quantum diffusion of the oscillating electron wavefunction results in a strong increase in the single-atom rescattering probability, and an associated increase in XUV flux. Since the single-atom HHG efficiency scales with the driving wavelength λ as λ^{-5}–λ^{-9} [37,52–54], frequency doubling of the driving laser already results in an increase of the single-atom yield by about two orders of magnitude [48]. Therefore, by using shorter wavelength driving lasers, the HHG process can be driven with very *moderate* intensities that are still sufficient to achieve *bright* harmonics. Using moderate intensities to drive the HHG process enables us to avoid previous detrimental side-effects (blue-shifting, self-phase modulation) that did lead to a considerably broader harmonic spectrum than expected from time-bandwidth product. As an added benefit, due to the shorter time the electron spends in the continuum, the electron motion and the high-harmonic bandwidth and peak positions are less sensitive to the plasma conditions. This results in a HHG spectrum that is more stable in brightness, spectral position and bandwidth.

Finally and most importantly for ARPES, since the single atom yield is much higher for shorter wavelength driving lasers, longer pulses can be used to generate harmonics while *still achieving good conversion efficiency*. Using longer driving laser pulses results in narrower band HHG peaks (c.f. Fig. 1). In other words, energy and time resolution can be fairly easily adjusted to the specific needs of the experiment. Therefore, using shorter driving wavelengths at moderate HHG pump intensities and pulse lengths, narrow-band, stable, spectrally separated and bright high-harmonic output can be simultaneously achieved.

3. Time-resolved ARPES with optimized and bright XUV pulses

Fig. 4 shows photoemission maps of the charge-density-wave material $TiSe_2$ from our previous work using 780 nm driving light for harmonic generation (left) [13,17] in comparison to our new data (right) using 390 nm driving laser. When comparing the electronic bands in the red marked area between the old and the new data, one clearly sees that the energy resolution is dramatically increased. In order to characterize the bandwidth of the

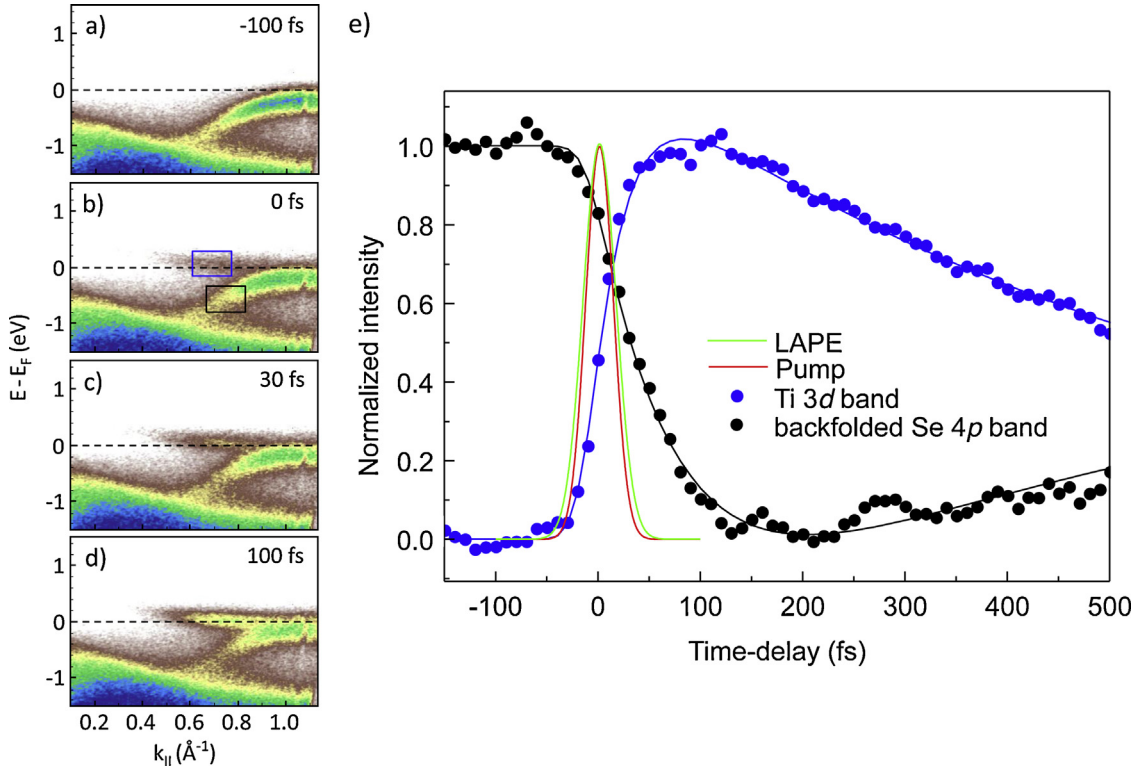

Fig. 5. Photo-induced electronic structure changes of $TiSe_2$. (a–d) Snapshots of the electronic structure as a function of pump-probe delay. (e) Extracted transient dynamics. The green line corresponds to the LAPE signal, which is equivalent to a cross-correlation of infrared pump and XUV probe pulse. The red line corresponds to the pulse duration of the infrared pump pulse. The black dots (extracted by integrating the photoemission intensity within the black rectangular area indicated in (b)) and black line (fit) show the transient intensity of the back-folded Se 4*p* bands to the M point, which is a signature of quenching of the charge-density-wave state in this system. The blue dots (extracted by integrating the photoemission intensity within the blue rectangular area indicated in (b)) and line (fit) correspond to the filling of the Ti 3*d* band. (For interpretation of the references to color in this text, the reader is referred to the web version of the article.)

individual harmonics, we carried out additional measurements using a narrow-bandwidth laser system and a He discharge lamp (not shown). By comparison, we extract values for the energy resolution that are <150 meV at optimal operation conditions (depending on chirp, HHG fiber alignment, and gas pressure). Note that the single harmonic bandwidth, and thereby the energy resolution, can further be improved by using even shorter wavelength driving lasers for the HHG process.

Similar to the progress in high-resolution static photoemission spectroscopy at synchrotrons [2], it is clear that such a dramatic improvement in energy resolution opens up real-time studies of a much larger range of applications. In particular in the case of correlated-electron materials, higher-resolution photoemission is required to resolve typical characteristic features in the electronic structure. Examples include various electronic order parameters, as for instance superconducting gaps, or quasiparticle kinks in the electronic dispersion relation.

Next, we note that typical integration times for spectra as shown in Fig. 4, right side, are below 10 s, in comparison to minutes in our previous works (Fig. 4, left). Clearly, the overall XUV photon output is higher, which is due to a combination of higher photon conversion efficiency at shorter wavelengths, elimination of monochromatizing optical elements, and less reabsorption in the gas due to a lower phase-matching pressure. In comparison to our previous work, where we had a photon flux of $\sim 1 \times 10^9$ photons/harmonic/second, we estimate the photon flux in the current presented setup to be nearly two orders of magnitude higher.

Finally, the question arises if the pulse length of the HHG is sufficiently short to not degrade our achievable time resolution. Here, we want to point out that most of the time-resolved ARPES experiments to date have used the fundamental laser pulse from the amplifier for pumping the material system, which is 20 fs or even longer (unless externally compressed). Consequently, the overall time resolution of the system is limited to that of the pump pulse, so the pulse length of the HHG needs only to be comparable or smaller than the pulse length of the pump pulse to maintain good time resolution.

Usually, the pulse length of the HHG can be measured using the laser-assisted photoelectric effect (LAPE), which corresponds to the cross-correlation of the infrared pump and the XUV probe pulse [55]. Note that for harmonic energies of about 22 eV and lower, the required pump intensities to generate LAPE sidebands are very high [56], i.e. the LAPE signal can be extracted from our raw data, but is hardly seen in the photoemission spectra presented in Fig. 5a–d. This is because the LAPE signal decreases with the kinetic energy of the photoemitted electrons [56]. The extracted LAPE signal from the raw data is fitted and plotted in Fig. 5e (green line) together with the pulse duration of the infrared pump pulse (red line), measured independently with frequency-resolved optical gating (FROG). The corresponding full widths at half maximum (FWHM) are 38 ± 8 fs for the cross-correlation and 32.0 ± 0.5 fs for the infrared pulse length. From this, we extract a pulse duration of the HHG of 20 ± 16 fs.

In addition to the LAPE measurement, we also verified our time resolution by reproducing the photo-induced semiconductor-to-metal transition in $TiSe_2$, which we characterized in an earlier study [13]. Fig. 5 shows a series of time-resolved photoemission spectra from $TiSe_2$ after excitation with a fluence of 1.3 mJ/cm^2. The extracted exponential time constant for the transition is about 51 ± 15 fs (black dots and line), which is in agreement with our previous investigation [13]. Most importantly, however, is the time constant for the filling of the Ti 3*d* band, which happens within 31 ± 3 fs (blue dots and line) and gives an upper limit for the time

resolution of our XUV *tr*ARPES setup. From these measurements, we therefore conclude that the time-resolution is still predominantly limited by the pulse length of the pump pulse rather than the HHG pulse.

4. Summary

In summary, we have shown that shorter wavelength driven HHG is well suited for *tr*ARPES. In particular, we have shown that 390 nm driven high harmonic XUV *tr*ARPES is much superior to using 790 nm laser drivers, because it eliminates the need for any spectral selection element, thereby increasing the photon flux and energy resolution (<150 meV here), while preserving excellent time resolution of about 30 fs. Using even shorter wavelength driving lasers will further increase the efficiency while decreasing the bandwidth of the individual harmonics [28,29]. Moreover, the current scheme can readily be implemented in higher repetition-rate laser systems with even longer pulse-lengths, and can be useful for other experimental XUV experiments, such as COLTRIMS, VMI, and magneto-optical setups.

Acknowledgements

A.R., S.M., M.A. acknowledge support from the German Science Foundation through Transregio SFB TR49. M.M., H.K., A.C., P.M. acknowledge support for this work from the NSF Physics Frontiers Centers. L.K., K.R., and M.B. acknowledge support from the German Science Foundation through grant DFG-BA 2177/9-1. S.J. is a recipient of a fellowship through the Excellence Initiative (DFG/GSC 266). P.M. acknowledges support from the Swedish Research Council (Vetenskapsrådet).

References

[1] A. Damascelli, Z. Hussain, Z.-X. Shen, Rev. Mod. Phys. 75 (2003) 473.
[2] F. Reinert, S. Hüfner, New J. Phys. 7 (2005) 97.
[3] J.H. Dil, J. Phys. Condens. Mater. 21 (2009) 403001.
[4] F. Schmitt, P.S. Kirchmann, U. Bovensiepen, R.G. Moore, L. Rettig, M. Krenz, J.H. Chu, N. Ru, L. Perfetti, D.H. Lu, M. Wolf, I.R. Fisher, Z.X. Shen, Science 321 (2008) 1649.
[5] U. Bovensiepen, P.S. Kirchmann, Laser Photon Rev. 6 (2012) 589.
[6] R. Cortés, L. Rettig, Y. Yoshida, H. Eisaki, M. Wolf, U. Bovensiepen, Phys. Rev. Lett. 107 (2011) 097002.
[7] L. Rettig, R. Cortés, S. Thirupathaiah, P. Gegenwart, H. Jeevan, M. Wolf, J. Fink, U. Bovensiepen, Phys. Rev. Lett. 108 (2012) 097002.
[8] C.L. Smallwood, J.P. Hinton, C. Jozwiak, W. Zhang, J.D. Koralek, H. Eisaki, D.H. Lee, J. Orenstein, A. Lanzara, Science 336 (2012) 1137.
[9] M. Seaberg, D. Adams, E. Townsend, D.A. Raymondson, W.F. Schlotter, Y. Liu, C.S. Menoni, L. Rong, C.-C. Chen, J. Miao, H.C. Kapteyn, M.M. Murnane, Opt. Express 19 (2011) 22470.
[10] R. Haight, J.A. Silberman, Phys. Rev. Lett. 62 (1989) 815.
[11] A.L. Cavalieri, N. Müller, T. Uphues, V.S. Yakovlev, A. Baltuška, B. Horvath, B. Schmidt, L. Blümel, R. Holzwarth, S. Hendel, M. Drescher, U. Kleineberg, P.M. Echenique, R. Kienberger, F. Krausz, U. Heinzmann, Nature 449 (2007) 1029.
[12] P. Siffalovic, M. Drescher, U. Heinzmann, Europhys. Lett. 60 (2002) 924.
[13] T. Rohwer, S. Hellmann, M. Wiesenmayer, C. Sohrt, A. Stange, B. Slomski, A. Carr, Y. Liu, L.M. Avila, M. Kallaene, S. Mathias, L. Kipp, K. Rossnagel, M. Bauer, Nature 471 (2011) 490.
[14] S. Hellmann, T. Rohwer, M. Kalläne, K. Hanff, C. Sohrt, A. Stange, A. Carr, M.M. Murnane, H.C. Kapteyn, L. Kipp, M. Bauer, K. Rossnagel, Nat. Commun. 3 (2012) 1069.
[15] J. Petersen, S. Kaiser, N. Dean, A. Simoncig, H. Liu, A. Cavalieri, C. Cacho, I. Turcu, E. Springate, F. Frassetto, L. Poletto, S. Dhesi, H. Berger, A. Cavalleri, Phys. Rev. Lett. 107 (2011) 177402.
[16] R. Carley, K. Döbrich, B. Frietsch, C. Gahl, M. Teichmann, O. Schwarzkopf, P. Wernet, M. Weinelt, Phys. Rev. Lett. 109 (2012) 057401.
[17] S. Mathias, L. Miaja-Avila, M.M. Murnane, H. Kapteyn, M. Aeschlimann, M. Bauer, Rev. Sci. Instrum. 78 (2007) 083105.
[18] S. Mathias, M. Bauer, M. Aeschlimann, L. Miaja-Avila, H.C. Kapteyn, M.M. Murnane, Time-Resolved Photoelectron Spectroscopy at Surfaces Using Femtosecond XUV Pulses, Wiley-VCH Verlag GmbH & Co. KGaA, Weinheim, Germany, 2010, pp. 499–535.
[19] G. Dakovski, Y. Li, S. Gilbertson, G. Rodriguez, A. Balatsky, J.-X. Zhu, K. Gofryk, E. Bauer, P. Tobash, A. Taylor, J. Sarrao, P. Oppeneer, P. Riseborough, J. Mydosh, T. Durakiewicz, Phys. Rev. B 84 (2011) 161103.
[20] H. Dachraoui, M. Michelswirth, P. Siffalovic, P. Bartz, C. Schaefer, B. Schnatwinkel, J. Mattay, W. Pfeiffer, M. Drescher, U. Heinzmann, Phys. Rev. Lett. 106 (2011).
[21] K. Ishizaka, T. Kiss, T. Yamamoto, Y. Ishida, T. Saitoh, M. Matsunami, R. Eguchi, T. Ohtsuki, A. Kosuge, T. Kanai, M. Nohara, H. Takagi, S. Watanabe, S. Shin, Phys. Rev. B 83 (2011) 081104.
[22] R. Haight, D.R. Peale, Rev. Sci. Instrum. 65 (1994) 1853.
[23] M. Bauer, C. Lei, K. Read, R. Tobey, J. Gland, M. Murnane, H. Kapteyn, Phys. Rev. Lett. 87 (2001) 025501.
[24] S. Mathias, M. Wiesenmayer, F. Deicke, A. Ruffing, L. Miaja-Avila, M.M. Murnane, H.C. Kapteyn, M. Bauer, M. Aeschlimann, J. Phys.: Conf. Ser. 148 (2009) 012042.
[25] M. Bauer, J. Phys. D: Appl. Phys. 38 (2005) R253.
[26] T. Haarlammert, H. Zacharias, Curr. Opin. Solid State Mater. 1 (2009).
[27] S.G. Preston, A. Sanpera, M. Zepf, W.J. Blyth, C.G. Smith, J.S. Wark, M.H. Key, K. Burnett, M. Nakai, D. Neely, Phys. Rev. A 53 (1996) R31.
[28] T. Popmintchev, M.-C. Chen, D. Popmintchev, P. Arpin, S. Brown, S. Alisauskas, G. Andriukaitis, T. Balciunas, O.D. Muecke, A. Pugzlys, A. Baltuska, B. Shim, S.E. Schrauth, A. Gaeta, C. Hernandez-Garcia, L. Plaja, A. Becker, A. Jaron-Becker, M.M. Murnane, H.C. Kapteyn, Science 336 (2012) 1287.
[29] T. Popmintchev, M.M. Murnane, H.C. Kapteyn, in preparation.
[30] R. Dörner, V. Mergel, O. Jagutzki, L. Spielberger, J. Ullrich, R. Moshammer, H. Schmidt-Böcking, Phys. Rep. 330 (2000) 95.
[31] J. Ullrich, R. Moshammer, A. Dorn, R. Dörner, L.P.H. Schmidt, H. Schmidt-Böcking, Rep. Prog. Phys. 66 (2003) 1463.
[32] E. Gagnon, A.S. Sandhu, A. Paul, K. Hagen, A. Czasch, T. Jahnke, P. Ranitovic, C. Lewis Cocke, B. Walker, M.M. Murnane, H.C. Kapteyn, Rev. Sci. Instrum. 79 (2008) 063102.
[33] A.T.J.B. Eppink, D.H. Parker, Rev. Sci. Instrum. 68 (1997) 3477.
[34] C. La-O-Vorakiat, M. Siemens, M.M. Murnane, H.C. Kapteyn, S. Mathias, M. Aeschlimann, P. Grychtol, R. Adam, C.M. Schneider, J.M. Shaw, H. Nembach, T.J. Silva, Phys. Rev. Lett. 103 (2009) 257402.
[35] S. Mathias, C. La-O-Vorakiat, J.M. Shaw, E. Turgut, P. Grychtol, R. Adam, D. Rudolf, H.T. Nembach, T.J. Silva, M. Aeschlimann, C.M. Schneider, H.C. Kapteyn, M.M. Murnane, J. Electron Spectrosc. Relat. Phenom. 189 (2013) 164.
[36] E. Turgut, C. La-o-vorakiat, J.M. Shaw, P. Grychtol, H.T. Nembach, D. Rudolf, R. Adam, M. Aeschlimann, C.M. Schneider, T.J. Silva, M.M. Murnane, H.C. Kapteyn, S. Mathias, Phys. Rev. Lett. 110 (2013) 197201.
[37] T. Popmintchev, M.-C. Chen, P. Arpin, M.M. Murnane, H.C. Kapteyn, Nat. Photon 4 (2010) 822.
[38] A. Rundquist, C.G. Durfee, Z. Chang, C. Herne, S. Backus, M.M. Murnane, H.C. Kapteyn, Science 280 (1998) 1412.
[39] R. Haight, D.R. Peale, Phys. Rev. Lett. 70 (1993) 3979.
[40] M. Bauer, C. Lei, R. Tobey, M.M. Murnane, H. Kapteyn, Surf. Sci. 532 (2003) 1159.
[41] R.L. Sandberg, A. Paul, D.A. Raymondson, S. Haedrich, D.M. Gaudiosi, J. Holtsnider, R.I. Tobey, O. Cohen, M.M. Murnane, H.C. Kapteyn, C. Song, J. Miao, Y. Liu, F. Salmassi, Phys. Rev. Lett. 99 (2007) 098103.
[42] I.C.E. Turcu, E. Springate, C.A. Froud, C.M. Cacho, J.L. Collier, W.A. Bryan, G.R.A.J. Nemeth, J.P. Marangos, J.W.G. Tisch, R. Torres, T. Siegel, L. Brugnera, J.G. Underwood, I. Procino, W.R. Newell, C. Altucci, R. Velotta, R.B. King, J.D. Alexander, C.R. Calvert, O. Kelly, J.B. Greenwood, I.D. Williams, A. Cavalleri, J.C. Petersen, N. Dean, S.S. Dhesi, L. Poletto, P. Villoresi, F. Frassetto, S. Bonora, M.D. Roper, Romopto 2009, in: V.I. Vlad (Ed.), SPIE, 2010, pp. 746902–746902-15.
[43] L. Poletto, P. Villoresi, F. Frassetto, F. Calegari, F. Ferrari, M. Lucchini, G. Sansone, M. Nisoli, Rev. Sci. Instrum. 80 (2009) 123109.
[44] S. Backus, R. Bartels, S. Thompson, R. Dollinger, H.C. Kapteyn, M.M. Murnane, Opt. Lett. 26 (2001) 465.
[45] J. Zhou, J. Peatross, M.M. Murnane, H.C. Kapteyn, I.P. Christov, Phys. Rev. Lett. 76 (1996) 752.
[46] H. Kapteyn, M. Murnane, I. Christov, Phys. Today 58 (2005) 39.
[47] B.L. Henke, E.M. Gullikson, J.C. Davis, Atom. Data Nucl. Data Tables 54 (1993) Tables.
[48] E.L. Falcão-Filho, C.-J. Lai, K.-H. Hong, V.-M. Gkortsas, S.-W. Huang, L.-J. Chen, F.X. Kärtner, Appl. Phys. Lett. 97 (2010) 061107.
[49] F. Shimizu, Phys. Rev. Lett. 19 (1967) 1097.
[50] W.M. Wood, C.W. Siders, M.C. Downer, Phys. Rev. Lett. 67 (1991) 3523.
[51] N. Wagner, E. Gibson, T. Popmintchev, I. Christov, M. Murnane, H. Kapteyn, Phys. Rev. Lett. 93 (2004) 173902.
[52] P.B. Corkum, Phys. Rev. Lett. 71 (1993) 1994.
[53] J. Tate, T. Auguste, H. Muller, P. Salieres, P. Agostini, L. DiMauro, Phys. Rev. Lett. 98 (2007) 013901.
[54] T. Popmintchev, M.-C. Chen, A. Bahabad, M. Gerrity, P. Sidorenko, O. Cohen, I.P. Christov, M.M. Murnane, H.C. Kapteyn, Proc. Natl. Acad. Sci. U. S. A. 106 (2009) 10516.
[55] L. Miaja-Avila, C. Lei, M. Aeschlimann, J.L. Gland, M.M. Murnane, H.C. Kapteyn, G. Saathoff, Phys. Rev. Lett. 97 (2006) 113604.
[56] G. Saathoff, L. Miaja-Avila, M. Aeschlimann, M.M. Murnane, H.C. Kapteyn, Phys. Rev. A 77 (2008) 022903.